Supporting Information

Enhanced corrosion resistance of carbon steel in hydrochloric acid solution by polyoxometalate-estertin derivatives

Xing-Fang Wang[1 #], Xin-Yu Liu[1 #], Fang Su[1], Jian-Sheng Li[1], Zai-Ming Zhu[1 *], Xiao-Jing Sang[1 *], and Lan-Cui Zhang[1 *]

[1] School of Chemistry and Chemical Engineering, Liaoning Normal University, Dalian, 116029, P.R. China.

[#] Xing-Fang Wang and Xin-Yu Liu are coauthors.

[*] Corresponding author.

CONTENTS

1. Synthesis

$Na_5K_5[(Sn(CH_2CH_2COO))_2(Ni(H_2O)_3)_2(B\text{-}\beta\text{-}BiW_9O_{33})_2]\cdot 20H_2O$ (BiW_9-Ni-SnR). Parent POM **Na-BiW_9** (0.288 g, 0.1 mmol), $Cl_3Sn(CH_2)_2COOCH_3$ (0.062 g, 0.2 mmol) and $Ni(NO_3)_2\cdot 6H_2O$ (0.087 g, 0.3 mmol) were dissolved in 10.0 mL of 0.4 M NaAc-HAc buffer solution (pH ≈ 5.0) to form solutions A, B and C, respectively. Then solution B was slowly added to solution A, and stirred at 80 °C for 1 h, and then solution C was added dropwise to the above mixed solution, and stirred for another 2 h. After cooling to room temperature, a certain amount of guanidine hydrochloride ($C(NH_2)_3Cl$) aqueous solution and KCl (s) were added to the obtained solution. Slow evaporation of the aqueous solution at 50 °C resulted in green block crystals (yield: ca. 52.3% based on **Na-BiW_9**) of **BiW_9-Ni-SnR** after about four days.

$Na_5K_5[(Sn(CH_2CH_2COO))_2(Zn(H_2O)_3)_2(B\text{-}\beta\text{-}BiW_9O_{33})_2]\cdot 21H_2O$ (BiW_9-Zn-SnR). The synthesis method of **BiW_9-Zn-SnR** was similar to that of **BiW_9-Ni-SnR** by replacing $Ni(NO_3)_2\cdot 6H_2O$ with $ZnCl_2$ (0.082 g, 0.6 mmol), and the mass of **Na-BiW_9** and $Cl_3SnCH_2CH_2COOCH_3$ were increased to 0.580 g (0.2 mmol) and 0.124 g (0.4 mmol), respectively. Finally, colorless block crystals were obtained (yield: ca. 53.0% based on **Na-BiW_9**).

Synthesis of SbW_9-TM-SnR (TM = Mn, Co, Ni, Zn) and **BiW_9-TM-SnR** (TM = Mn, Co)

These six inorganic-organic hybrid sandwich-type tungstoantimonates/tungstobismuthates, i.e. **SbW_9-TM-SnR** (TM = Mn, Co, Ni, Zn) and **BiW_9-TM-SnR** (TM = Mn, Co), were synthesized and characterized according to the methods reported in our previous work.[1, 2]

Discussion on synthesis methods

Two new sandwich-type POMs **BiW_9-Ni-SnR** and **BiW_9-Zn-SnR** were obtained with conventional synthesis method (Scheme S1). As shown in Scheme S1, H_2O was initially selected as a solvent, and the raw materials **Na-BiW_9**, $Cl_3SnCH_2CH_2COOCH_3$ and $Ni(NO_3)_2\cdot 6H_2O$ were added. As a result, using the "one-pot" synthesis method, the solution became turbid and crystals could not grow. Considering the sensitivity of POMs to pH and our research team's previous experience in the synthesis of such compounds, it may be suitable for crystal growth under a certain acidity environment, so NaAc-HAc buffer solution was chosen as a solvent. In the buffer range of pH = 4–5.5, crystals can successfully grow. Under the same optimum synthetic conditions as those of **BiW_9-Ni-SnR**, crystalline **BiW_9-Zn-SnR** with the same polyoxoanion skeleton was obtained by replacing the Ni^{2+} salt with $ZnCl_2$, and doubling the amount of substance of all reactants.

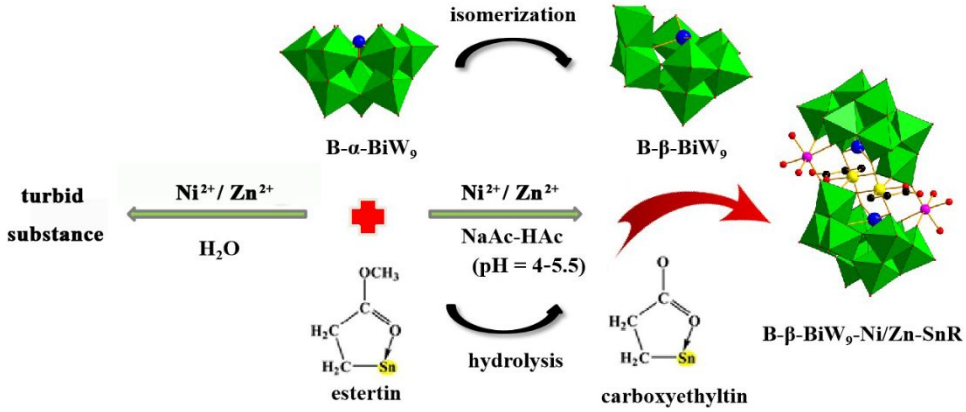

Scheme S1 The formation process of inhibitors **BiW_9-Ni-SnR** and **BiW_9-Zn-SnR**

2. CHARACTERIZATION

2.1 X-ray crystallography and structural analysis

Using Mo Kα ray (λ = 0.071073 nm) as the radiation source, the two high-quality crystalline POMs **BiW_9-Ni-SnR** and **BiW_9-Zn-SnR** were selected for single crystal X-ray diffraction test, and to collect crystal data on the Bruker smart apex II single crystal diffractometer. Using SHELXTL-2014 crystallographic software,[3] the structures of **BiW_9-Ni-SnR** and **BiW_9-Zn-SnR** were solved and refined with direct methods and full-matrix least-squares fitting on F^2, respectively, and an empirical absorption correction was applied using the SADABS program. All H atoms on C atoms were added according to the calculated positions, and H atoms in H_2O molecules were directly added in the molecular formulas. Table S1 listed the crystal data and structure refinement of the two POMs. Their selected bond lengths and angles are shown in Tables S2−S3. Their CCDC reference number: 2069049 and 2069050.

Table S1 Crystal and refinement data for **BiW_9-Ni-SnR** and **BiW_9-Zn-SnR**

Compound	**BiW_9-Ni-SnR**	**BiW_9-Zn-SnR**
Formula	$C_6H_{60}K_5Na_5O_{96}Bi_2Ni_2Sn_2W_{18}$	$C_6H_{62}K_5Na_5O_{97}Bi_2Zn_2Sn_2W_{18}$
Formula weight	6061.05	6092.38
T/K	296(2)	296(2)
Wavelength/nm	0.071073	0.071073
Crystal system	Triclinic	Triclinic
Space group	*P*$\bar{1}$	*P*$\bar{1}$
a/nm	1.2391(4)	1.2394(2)
b/nm	1.2538(4)	1.2575(2)

c/nm	1.6264(5)	1.6329(3)
α/°	95.314(5)	94.652(3)
β/°	110.009(5)	109.921(3)
γ/°	101.548(5)	101.956(3)
V/nm^3, Z	2.2904(11), 1	2.3087(7), 1
D_c/g cm^{-3}, F_{000}	4.394, 2668	4.382, 2682
GOF	1.000	1.023
Reflections collected	11406	11965
R_{int}	0.0458	0.0302
θ Range (°)	1.353−24.996	1.678−25.000
R_1 ($I > 2\sigma(I)$)[a]	0.0511	0.0396
wR_2 (all data)[a]	0.1325	0.1026

[a] $R_1 = \sum||F_0|-|F_C||/\sum|F_0|$; $wR_2 = \sum[w(F_0^2-F_C^2)^2]/\sum[w(F_0^2)^2]^{1/2}$

2.2 Selected bond lengths and angles

Table S2 Selected bond lengths (nm) and angles (°) for **BiW_9-Ni-SnR**

Bond	Length (nm)	Bond	Length (nm)	Bond	Length (nm)
W1–O12	0.1737(15)	W5–O29	0.1858(16)	W9–O1	0.1907(12)
W1–O16	0.1772(15)	W5–O4	0.1917(14)	W9–O3	0.1908(14)
W1–O11	0.1918(15)	W5–O2	0.1932(13)	W9–O17	0.1952(13)
W1–O5	0.1949(14)	W5–O6	0.1954(14)	W9–O21	0.2269(13)
W1–O19	0.2071(16)	W5–O20	0.2232(14)	Bi1–O21	0.2088(14)
W1–O22	0.2188(14)	W6–O28	0.1701(14)	Bi1–O20	0.2141(13)
W2–O14	0.1720(14)	W6–O25	0.1856(14)	Bi1–O22	0.2161(12)
W2–O24	0.1796(14)	W6–O30	0.1891(13)	Sn1–O23	0.2050(15)
W2–O23	0.1799(14)	W6–O6	0.1937(14)	Sn1–O24#3	0.2062(14)
W2–O1	0.1963(14)	W6–O33	0.1984(14)	Sn1–O25#3	0.2071(14)
W2–O18	0.2017(14)	W6–O20	0.2243(13)	Sn1–O26	0.2089(13)
W2–O21	0.2218(12)	W7–O31	0.1730(15)	Sn1–C1	0.208(2)
W3–O8	0.1707(15)	W7–O15	0.1773(15)	Sn1–O34	0.2152(15)
W3–O33	0.1825 (14)	W7–O11	0.1903(15)	Ni1–O3W	0.203(2)
W3–O18	0.1862(13)	W7–O30	0.1979(13)	Ni1–O2W	0.203(2)
W3–O3	0.1918(14)	W7–O29	0.2026(17)	Ni1–O16	0.2036(16)
W3–O2	0.1931(13)	W7–O20	0.2197(14)	Ni1–O15	0.2050(16)
W3–O21	0.2337(13)	W8–O9	0.1739(15)	Ni1–O14#3	0.2085(14)

W4–O32	0.1725(15)	W8–O26	0.1836(13)	Ni1–O1W	0.2103(18)
W4–O19	0.1860(16)	W8–O5	0.1922(14)	C3–O34	0.129(3)
W4–O4	0.1894(15)	W8–O7	0.1942(12)	C3–O35	0.122(3)
W4–O17	0.1898(14)	W8–O10	0.1955(14)	C1–C2	0.1507(10)
W4–O7	0.1933(13)	W8–O22	0.2229(14)	C2–C3	0.1511(10)
W4–O22	0.2222(13)	W9–O13	0.1695(15)		
W5–O27	0.1705(14)	W9–O10	0.1887(14)		
Bond	**Angle(°)**	**Bond**	**Angle(°)**	**Bond**	**Angle(°)**
O11–W1–O5	161.3(6)	O4–W5–O6	164.8(6)	O1–W9–O17	161.8(6)
O16–W1–O19	161.5(7)	O27–W5–O20	171.1(6)	O13–W9–O21	168.8(6)
O5–W1–O22	74.5(5)	O29–W5–O20	72.9(6)	O1–W9–O21	73.1(5)
O19–W1–O22	72.0(5)	O6–W5–O20	76.4(5)	O3–W9–O21	75.1(5)
O23–W2–O18	160.4(6)	O30–W6–O33	157.9(5)	O21–Bi1–O20	90.0(5)
O14–W2–O21	166.6(7)	O28–W6–O20	173.4(6)	O21–Bi1–O22	86.5(5)
O1–W2–O21	73.4(5)	O30–W6–O20	75.1(5)	O20–Bi1–O22	84.0(5)
O18–W2–O21	72.5(5)	O6–W6–O20	76.4(6)	O23–Sn1–C1	167.2(6)
O18–W3–O2	158.5(6)	O11–W7–O30	160.7(6)	O24#3–Sn1–O34	169.6(6)
O8–W3–O21	167.4(6)	O31–W7–O20	161.9(7)	O23–Sn1–O25#3	82.8(5)
O18–W3–O21	72.4(5)	O30–W7–O20	74.5(5)	C1–Sn1–O34	83.0(6)
O3–W3–O21	73.4(6)	O29–W7–O20	70.8(5)	O2W–Ni1–O16	174.3(8)
O4–W4–O7	162.2(6)	O5–W8–O10	159.0(6)	O3W–Ni1–O15	173.8(9)
O32–W4–O22	171.9(6)	O9–W8–O22	170.3(6)	O16–Ni1–O15	81.5(7)
O19–W4–O22	75.1(6)	O5–W8–O22	74.0(5)	O2W–Ni1–O14#3	85.2(7)
O7–W4–O22	74.4(5)	O7–W8–O22	74.1(5)		

Symmetry transformations used to generate equivalent atoms: #3 –x+2, –y+2, –z+1

Table S3 Selected bond lengths (nm) and angles (º) for **BiW_9-Zn-SnR**

Bond	**Length (nm)**	**Bond**	**Length (nm)**	**Bond**	**Length (nm)**
W1–O14	0.1754(10)	W5–O26	0.1862(10)	W9–O11	0.1911(10)
W1–O24	0.1815(9)	W5–O33	0.1904 (10)	W9–O10	0.1912(9)
W1–O23	0.1825(9)	W5–O30	0.1943(10)	W9–O3	0.1932(9)
W1–O11	0.1995(9)	W5–O13	0.1997(9)	W9–O22	0.2293(8)
W1–O7	0.2035(9)	W5–O21	0.2275(9)	Bi1–O22	0.2109(8)
W1–O22	0.2233(9)	W6–O27	0.1707(10)	Bi1–O21	0.2144(9)
W2–O1	0.1728(10)	W6–O31	0.1861 (9)	Bi1–O20	0.2158(9)
W2–O16	0.1764(11)	W6–O17	0.1911(9)	Sn1–O24#3	0.2047(10)

W2–O12	0.1942(9)	W6–O9	0.1917(9)	Sn1–O23	0.2057(9)
W2–O32	0.1967(9)	W6–O30	0.1942(10)	Sn1–O26	0.2092(10)
W2–O18	0.2068(10)	W6–O21	0.2248(10)	Sn1–O25#3	0.2110 (9)
W2–O20	0.2189 (9)	W7–O19	0.1736(11)	Sn1–C1	0.2112(13)
W3–O8	0.1733(9)	W7–O18	0.1880(9)	Sn1–O34	0.2162(9)
W3–O13	0.1851(9)	W7–O9	0.1907(9)	Zn1–O1W	0.2014(14)
W3–O7	0.1874(10)	W7–O3	0.1918 (9)	Zn1–O3W	0.2071(13)
W3–O10	0.1946(9)	W7–O5	0.1965(9)	Zn1–O16	0.2079(11)
W3–O17	0.1953(10)	W7–O20	0.2243(9)	Zn1–O15	0.2090(10)
W3–O22	0.2331(9)	W8–O6	0.1715(9)	Zn1–O14#1	0.2113(10)
W4–O28	0.1713(9)	W8–O25	0.1835(10)	Zn1–O2W	0.2151(13)
W4–O15	0.1768(11)	W8–O32	0.1925(9)	C3–O34	0.1279(16)
W4–O12	0.1894(10)	W8–O5	0.1964(10)	C3–O35	0.1248(16)
W4–O33	0.1993(9)	W8–O2	0.1965(9)	C1–C2	0.1536 (2)
W4–O31	0.2081(10)	W8–O20	0.2265(8)	C2–C3	0.149 (2)
W4–O21	0.2201(9)	W9–O4	0.1724 (9)		
W5–O29	0.1715(9)	W9–O2	0.1900(10)		
Bond	**Angle(°)**	**Bond**	**Angle(°)**	**Bond**	**Angle(°)**
O24–W1–O7	161.1(4)	O33–W5–O13	158.3(4)	O11–W9–O3	161.4(4)
O14–W1–O22	165.8(4)	O29–W5–O21	173.1(4)	O4–W9–O22	169.1(4)
O11–W1–O22	73.6(3)	O33–W5–O21	75.0(3)	O11–W9–O22	73.8(3)
O7–W1–O22	72.3(4)	O30–W5–O21	75.6(4)	O10–W9–O22	75.0(3)
O12–W2–O32	161.3(4)	O9–W6–O30	164.4(4)	O22–Bi1–O21	90.0(3)
O1–W2–O20	165.0(5)	O27–W6–O21	171.6(4)	O22–Bi1–O20	86.9(3)
O32–W2–O20	74.8(3)	O31–W6–O21	74.2(4)	O21–Bi1–O20	83.3(3)
O18–W2–O20	72.1(4)	O30–W6–O21	76.2(4)	O24#3–Sn1–C1	166.8(5)
O13–W3–O10	159.2(4)	O9–W7–O5	162.4(4)	O23–Sn1–O34	169.4(4)
O8–W3–O22	167.4(4)	O19–W7–O20	172.2(4)	O24#3–Sn1–O25#3	83.1(4)
O7–W3–O22	72.8(3)	O18–W7–O20	74.3(4)	C1–Sn1–O34	82.7(5)
O10–W3–O22	73.5(3)	O5–W7–O20	75.5(4)	O1W–Zn1–O15	172.2(6)
O12–W4–O33	161.1(4)	O32–W8–O2	159.3(4)	O14#3–Zn1–O2W	171.6(5)
O28–W4–O21	162.4(4)	O6–W8–O20	170.3(4)	O16–Zn1–O15	79.0(4)
O33–W4–O21	75.0(3)	O32–W8–O20	73.8(3)	O3W–Zn1–O14#3	83.5(5)
O31–W4–O21	71.4(4)	O5–W8–O20	75.1(3)		

Symmetry transformations used to generate equivalent atoms: #3 -x+1,-y+2,-z

2.3 Crystallographic structures

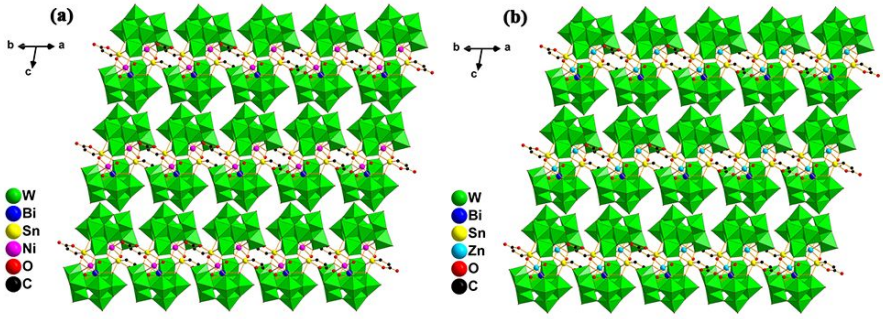

Figure S1 The packing arrangements of the polyoxoanions in **BiW$_9$-Ni-SnR** (a) and **BiW$_9$-Zn-SnR** (b) (all H atoms, K and Na cations, and free water molecules are omitted for clarity)

2.4 Physical characterizations

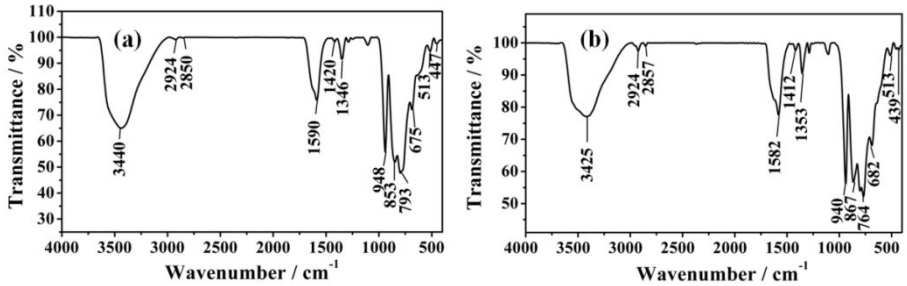

Figure S2 IR spectra of **BiW$_9$-Ni-SnR** (a) and **BiW$_9$-Zn-SnR** (b)

The IR spectra were performed on a Bruker AXS TENSOR-27 spectrophotometer in the range 400–4000 cm^{-1} (KBr pellets, POM: KBr = 1: 100). As shown in Figure S2, the vibration peaks between 950 and 670 cm^{-1} are attributed to ν(W−O$_t$), ν(Bi−O$_a$), ν(W−O$_b$) and ν(W−O$_c$) (O$_t$, O$_a$, O$_b$ and O$_c$ are terminal, tetrahedral, edge- and corner-sharing oxygen atoms).[4, 5] The peaks at 513/513 cm^{-1} and 447/439 cm^{-1} are antisymmetric and symmetric stretching vibrations of Sn–C bonds.[6] The peaks appearing at around 1590/1582 cm^{-1} and 1346/1353 cm^{-1} correspond to ν_{as}(COO) and ν_s(COO) vibrations, respectively.[7] The broad bands of lattice water molecules are located at 3440/3425 cm^{-1}. The peaks at 2924/2924 and 2850/2857 cm^{-1} are attributed to the characteristic vibrations of the organic group (–CH$_2$).[8]

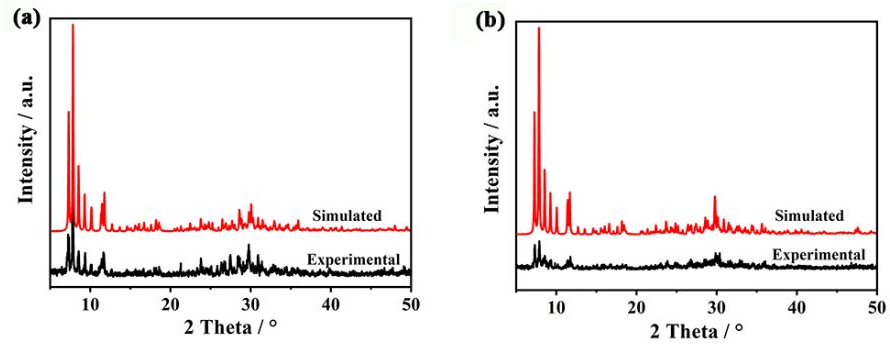

Figure S3 The simulated and experimental XRPD patterns of **BiW$_9$-Ni-SnR** (a) and **BiW$_9$-Zn-SnR** (b)

X-ray powder diffraction (PXRD) data was conducted on a Bruker AXS D8 Advance diffractometer using Cu Kα radiation (λ = 0.15418 nm) in the 2θ range of 5−50°. The fitting XRPD data (Simulated) obtained from the analysis of single crystal test was calculated by software, which was compared with the actual experimental values (Experimental). It can be seen from Figure S3 that the simulated and experimental values of **BiW_9-Ni-SnR** (a)/**BiW_9-Zn-SnR** (b) are in good agreement with each other, indicating that the two compounds are pure phase. Some differences in diffraction peak intensity may be due to the destruction of crystal water and the change of surface morphology.

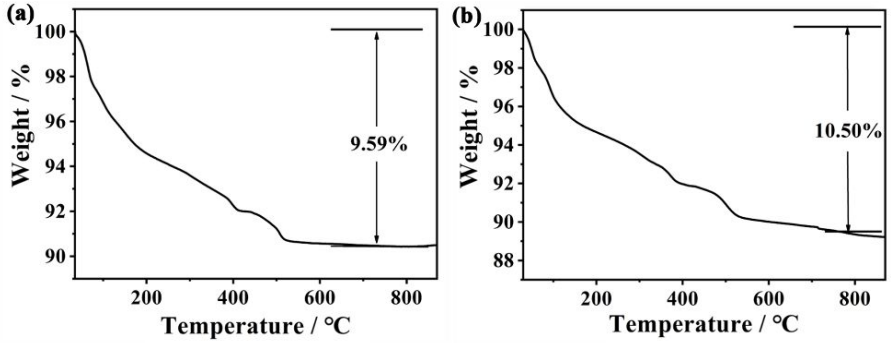

Figure S4 TG curves of **BiW_9-Ni-SnR** (a) and **BiW_9-Zn-SnR** (b)

Thermogravimetric (TG) measurement was measured on a Pyris Diamond TG-GTA thermal analyzer under air atmosphere with a heating rate of 10 ℃ min^{-1}. As presented in Figure S4, the TG curves of the two POMs show a similar three-step continuous weight loss from 30 to 800 °C. The total weight losses are 9.59% and 10.50% for **BiW_9-Ni-SnR** (a) and **BiW_9-Zn-SnR** (b), which correspond with the theoretical values of 10.09% and 10.32%, respectively. As can been seen from Figure S4a and b, the first weight losses of 5.95% (calcd 5.94%) and 6.49% (calcd 6.19%) in the ranges of 36–252 and 30–303 ℃ are ascribed to the loss of crystalline water molecules, respectively. The last two steps of weight losses of 3.64% and 4.01% (the calculated values are 4.15% and 4.13%) can be attributed to the loss of coordination water molecules and CH_2CH_2COO groups in the temperature range of 252–780 ℃ and 303–770 ℃ for **BiW_9-Ni-SnR** and **BiW_9-Zn-SnR**, respectively. It is obvious that the actual weight loss of **BiW_9-Ni-SnR** is lower than the theoretical weight loss, which may be caused by the partial loss of CH_2CH_2COO.

3. Corrosion inhibition performance

Table S4 Corrosion parameters obtained from weight loss measurement for 20# carbon steel immersed in 0.5 M HCl solution containing **Na-SbW$_9$** or **Na-BiW$_9$** for 6 and 10 h at 301 K

Inhibitor	Inhibitor concentration (mg L^{-1})	Time (h)	Δm (g)	C_R (mg cm^{-2} h^{-1})	IE$_w$ (%)
Na-SbW$_9$	300	6	0.0509	0.673	2.1
		10	0.0897	0.712	1.6
	500	6	0.0538	0.713	–
Na-BiW$_9$	300	6	0.0495	0.655	5.0
		10	0.0889	0.706	–
	500	6	0.0483	0.639	15.0

Table S5 Corrosion parameters derived from potentiodynamic polarization curves of 20# carbon steel in 1.0 M and 2.0 M HCl solutions in the absence (blank) and in the presence of inhibitors at 298 K

Inhibitor	HCl solution concentration (M)	β_a (mV dec^{-1})	β_c (mV dec^{-1})	E_{corr} (V *vs.* SCE)	I_{corr} (μA cm^{-2})	IE$_i$ (%)
Blank	1.0	85.7	-115.7	-0.202	509.8	–
	2.0	82.4	-107.1	-0.180	566.1	–
SbW$_9$-Mn-SnR	1.0	119.4	-141.7	-0.164	52.4	89.7
	2.0	74.3	-134.6	-0.166	70.0	87.6
SbW$_9$-Co-SnR	1.0	83.2	-134.4	-0.162	58.8	88.5
	2.0	89.0	-133.5	-0.155	66.5	88.2
SbW$_9$-Ni-SnR	1.0	87.0	-134.5	-0.159	60.1	88.2
	2.0	110.5	-135.3	-0.161	60.9	89.2
SbW$_9$-Zn-SnR	1.0	90.4	-136.8	-0.155	56.5	88.9
	2.0	100.5	-136.8	-0.165	63.6	88.8
BiW$_9$-Mn-SnR	1.0	90.9	-135.9	-0.167	58.2	88.6
	2.0	85.1	-131.8	-0.160	69.8	87.7
BiW$_9$-Co-SnR	1.0	90.6	-135.1	-0.173	56.7	88.9
	2.0	88.7	-136.0	-0.165	66.8	88.2
BiW$_9$-Ni-SnR	1.0	90.3	-132.4	-0.168	55.3	89.2
	2.0	89.5	-135.5	-0.171	63.2	88.8

BiW_9-Zn-SnR	1.0	101.2	-132.0	-0.168	47.2	90.7
	2.0	73.1	-138.3	-0.156	69.0	87.8
Na-SbW_9	1.0	59.3	-114.8	-0.197	192.5	62.2
	2.0	63.7	-120.2	-0.144	163.9	71.0
Na-BiW_9	1.0	72.2	-108.1	-0.209	154.6	69.7
	2.0	64.6	-114.9	-0.150	194.7	65.6
$Cl_3Sn(CH_2)_2COOCH_3$	1.0	103.6	-134.1	-0.181	77.3	84.8
	2.0	74,4	-134.3	-0.145	70.2	87.6

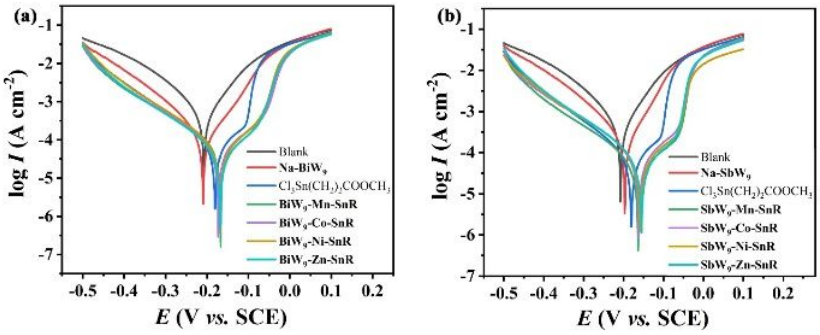

Figure S5 Potentiodynamic polarization curves for 20# carbon steel in 1.0 M HCl solution containing 150 mg L^{-1} of **Na-SbW_9/Na-BiW_9**, $Cl_3Sn(CH_2)_2COOCH_3$**, SbW_9-TM-SnR/BiW_9-TM-SnR** (TM = Mn, Co, Ni, Zn) corrosion inhibitor (a, b) at 298K. 1.0 M HCl solution was used as the blank

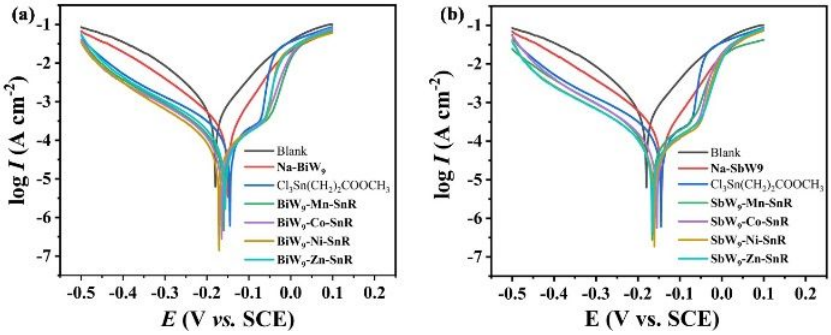

Figure S6 Potentiodynamic polarization curves for 20# carbon steel in 2.0 M HCl solution containing 150 mg L^{-1} of **Na-SbW_9/Na-BiW_9**, $Cl_3Sn(CH_2)_2COOCH_3$**, SbW_9-TM-SnR/BiW_9-TM-SnR** (TM = Mn, Co, Ni, Zn) corrosion inhibitor (a, b) at 298K. 2.0 M HCl solution was used as the blank

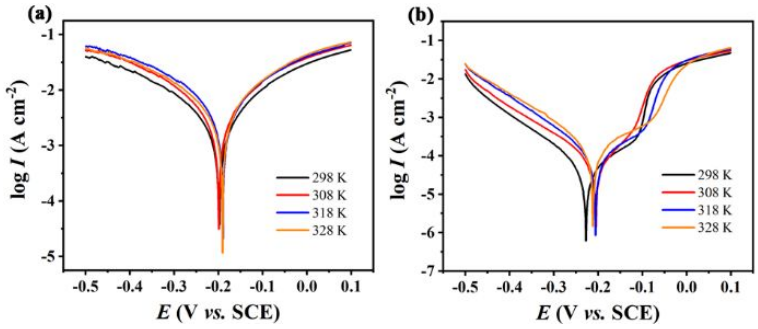

Figure S7 Potentiodynamic polarization curves for 20# carbon steel in 0.5 M HCl solution in the absence (a) and presence of **SbW$_9$-Mn-SnR** (b) at different temperatures

Table S6 Corrosion parameters derived from potentiodynamic polarization curves of 20# carbon steel in 0.5 M HCl solution in the absence (blank) and presence of **SbW$_9$-Mn-SnR** at different temperatures

Inhibitor	Temperature (K)	β_a (mV dec^{-1})	β_c (mV dec^{-1})	E_{corr} (V *vs.* SCE)	I_{corr} (μA cm^{-2})	IE$_i$ (%)
Blank	298	88.8	–135.6	–0.233	1096.5	–
	308	119.6	–149.5	–0.199	1216.2	–
	318	130.5	–143.5	–0.190	1391.3	–
	328	108.6	–133.4	–0.191	1584.9	–
SbW$_9$-Mn-SnR	298	80.9	–75.1	–0.228	43.8	96.0
	308	76.7	–119.7	–0.205	61.0	94.3
	318	85.8	–72.3	–0.206	86.8	93.8
	328	89.2	–69.3	–0.212	122.2	92.3

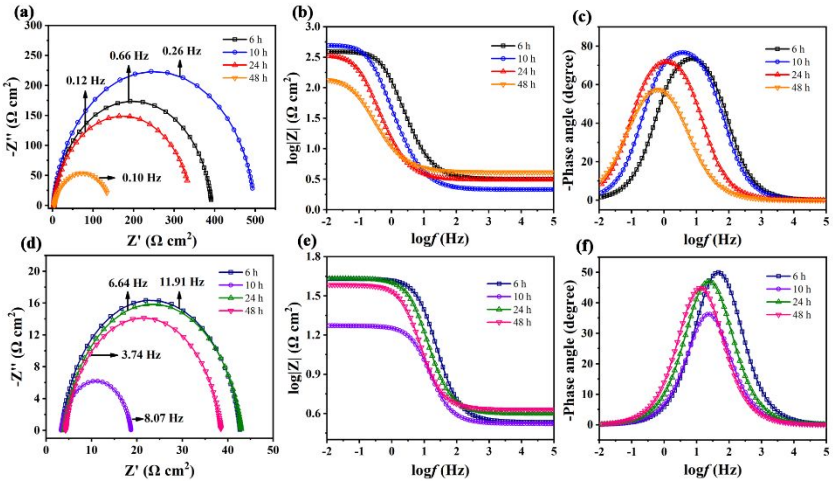

Figure S8 Nyquist plots, Bode Modulus plots and Bode Phase plots of 20# carbon steel immersed in 0.5 M HCl solution in presence of 150 mg L^{-1} **SbW$_9$-Mn-SnR** inhibitor (a, b, c) and the absence (d, e, f) for 6, 10, 24, 48 h at room temperature, respectively (Solid line shows fitted results)

4. Adsorption isotherm

The adsorption of corrosion inhibitors on the metal surface was determined by the use of different isotherms i.e., Frumkin, Freundlich, Temkin, Flory-Huggins and El-Awady adsorption isotherms. The following equations represented the adsorption isotherms:

Frumkin adsorption isotherm:

$$K_{ads}\, C_{\text{inh}} = \left(\frac{\theta}{1-\theta}\right) \exp(2\alpha\theta)$$

Freundlich adsorption isotherm:

$$\log K_{\text{ads}} + x\log C_{\text{inh}} = \ln\theta$$

Temkin adsorption isotherm:

$$K_{\text{ads}}\, C_{\text{inh}} = \exp(-2\alpha\theta)$$

El-Awady adsorption isotherm:

$$\ln K_{\text{ads}} + y\ln C_{\text{inh}} = \ln\left(\frac{\theta}{1-\theta}\right)$$

Flory-Huggins adsorption isotherm:

$$\ln z K_{\text{ads}} + z\ln(1-\theta) = \ln\left(\frac{\theta}{C_{\text{inh}}}\right)$$

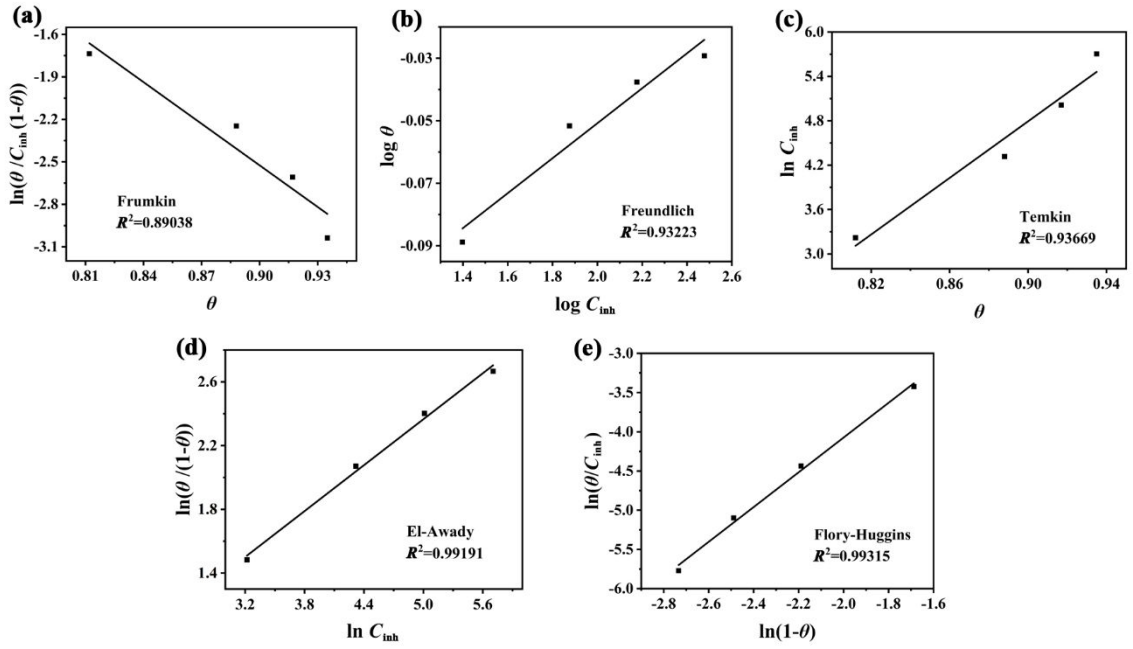

Figure S9 (a) Frumkin, (b) Freundlich, (c) Temkin, (d) El-Awady and (e) Flory-Huggins adsorption isotherms of **SbW_9-Mn-SnR** on 20# carbon steel in 0.5 M HCl solution at 298 K

5. Stability analysis of corrosion inhibitor

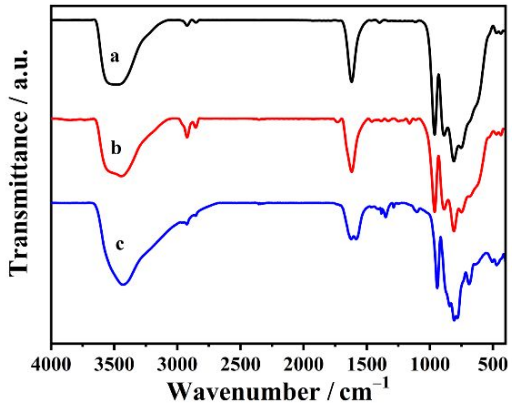

Figure S10 IR spectra of the solid sample obtained by recrystallization from the filtrate of 0.5 M HCl solution containing 150 mg L^{-1} **SbW_9-Mn-SnR** and excessive Fe powder for 6 h (a), the solid sample obtained by recrystallization after dissolving **SbW_9-Mn-SnR** in 0.5 M HCl solution for 6 h (b), and pure crystal **SbW_9-Mn-SnR** (c)

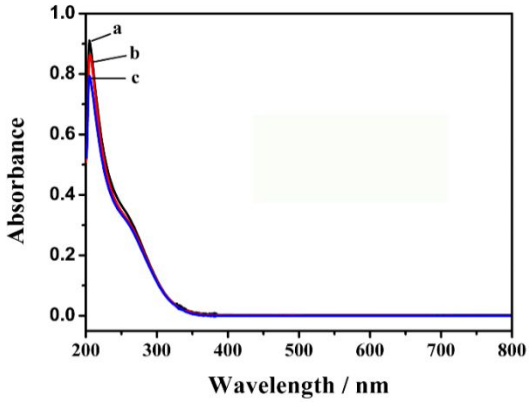

Figure S11 UV-vis absorption spectra of **SbW_9-Mn-SnR** dissolved in 0.5 M HCl solution for 0 h (a), 6 h (b), and 6 h with adding Fe powder (c)

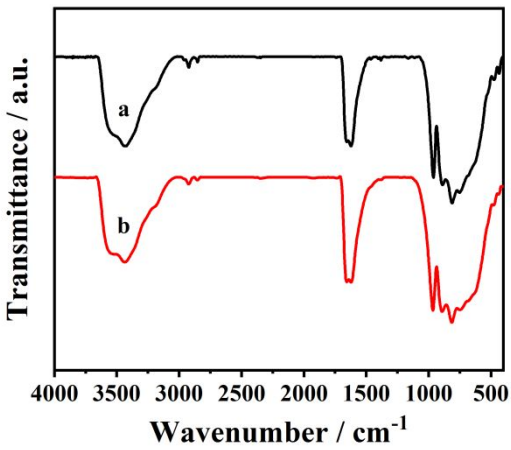

Figure S12 IR spectra of the solid sample obtained by recrystallization from the filtrate of 1.0 M (a) and 2.0 M (b) HCl solutions containing **SbW_9-Mn-SnR** and excessive Fe powder for 6 h

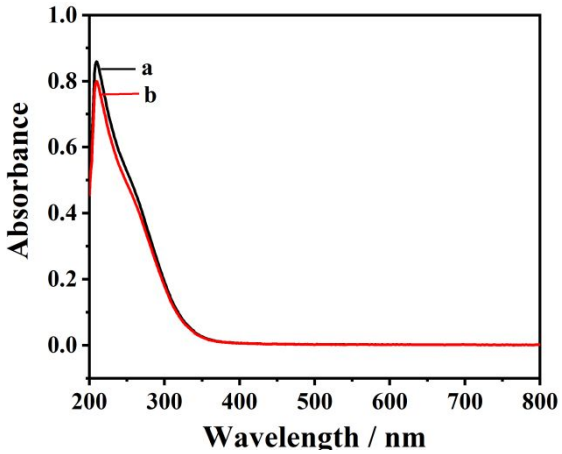

Figure S13 UV-vis absorption spectra of **SbW_9-Mn-SnR** dissolved in 1.0 M (a) and 2.0 M (b) HCl solutions for 6 h with adding Fe powder

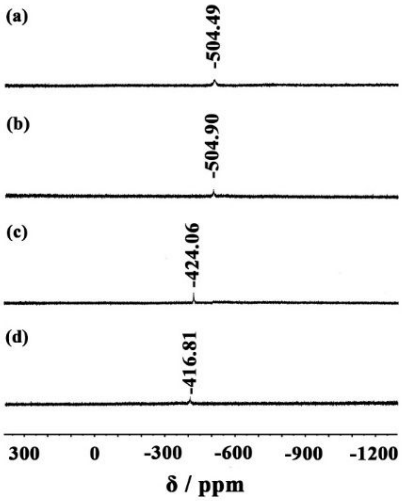

Figure S14 ^{119}Sn NMR spectra of **SbW_9-Co-SnR** in 0.5 M (a), 1.0 M (b) and 2.0 M (c) HCl solutions and ^{119}Sn NMR spectrum of $Cl_3Sn(CH_2)_2COOCH_3$ (d)

REFERENCES

(1) Wang, H. D.; Wang, X. F.; Su, F.; Li, J. S.; Zhang, L. C.; Sang, X. J.; Zhu, Z. M., Carboxyethyltin and transition metal co-functionalized tungstoantimonates composited with polypyrrole for enhanced electrocatalytic methanol oxidation. *Dalton Trans*. **2019**, *48*, 2977–2987. DOI 10.1039/c8dt05118f.

(2) Wang, Z. J.; Zhang, L. C.; Zhu, Z. M.; Chen, W. L.; You, W. S.; Wang, E. B., Two new sandwich-type tungstobismuthates constructed from trivacant Keggin units, estertin and transition metals. *Inorg. Chem. Commun*. **2012**, *17*, 151–154. DOI 10.1016/j.inoche.2011.12.038.

(3) Sheldrick, G. M.; Crystal structure refinement with SHELXL. *Acta Cryst*. **2015**, *C71*, 3–8. DOI 10.1107/S2053229614024218.

(4) Sun, C. Y.; Liu, S. X.; Wang, C. L.; Xie, L. H.; Zhang, C. D.; Gao, B.; Wang, E. B., Reactions of trivacant lone-paircontaining tungstobismutate and electrochemical behaviors of its sandwich-type products. *J. Coord. Chem*. **2007**, *60*, 567–579. DOI 10.1080/00958970600894972.

(5) Alizadeh, M. H.; Mohadeszadeh, M., Sandwich-type uranium-substituted of bismuthotungstate: synthesis and structure determination of $(Na(UO_2)_2(H_2O)_4(BiW_9O_{33})_2)^{13-}$. *J. Cluster Sci*. **2008**, *19*, 435–443. DOI 10.1007/s10876-008-0184-7.

(6) Khawar Raufa, M.; Adeel Saeeda, M.; Imtiaz-ud-Dina; Bolteb, M.; Badshaha, A.; Mirza, B., Synthesis, characterization and biological activities of some new organotin(IV) derivatives: crystal structure of $((SnPh_3)(OOCC_6H_4OH))$ and $((SnMe_3)_2(OOC)_2C_6Cl_4(DMSO)_2)$. *J. Organomet. Chem*. **2008**, *693*, 3043**–**3048. DOI 10.1016/j.jorganchem.2008.06.027.

(7) Deacon, G. B.; Phillips, R. J., Relationships between the carbon-oxygen stretching frequencies of carboxylato complexes and the type of carboxylate coordination. *Coord. Chem. Rev.* **1980**, *33*, 227–250. DOI 10.1016/S0010-8545(00)80455-5.

(8) Yang, G. Y.; Sevov, S. C., $[Co(en)_3][B_2P_3O_{11}(OH)_2]$: A novel borophosphate templated by a transition-metal complex. *Inorg. Chem.* **2001**, *40*, 2214–2215. DOI 10.1021/ic001397a.